The renal inflammatory network of nephronophthisis

Marceau Quatredeniers, Frank Bienaimé, Giulia Ferri, Pierre Isnard, Esther Porée, Katy Billot, Eléonore Birgy, Manal Mazloum, Salomé Ceccarelli, Flora Silbermann, et al.

The renal inflammatory network of nephronophthisis.

Marceau Quatredeniers[1], Frank Bienaimé[2,3,4], Giulia Ferri[1], Pierre Isnard[3,4,5], Esther Porée[1], Katy Billot[1], Eléonore Birgy[1], Manal Mazloum[4], Salomé Ceccarelli[1], Flora Silbermann[1], Simone Braeg[6], Thao Nguyen-Khoa[4,7], Rémi Salomon[1,3,8], Marie-Claire Gubler[1], E. Wolfgang Kuehn[6,9,10], Sophie Saunier[1], Amandine Viau[1,*].

Author Affiliations

[1] Université de Paris, Imagine Institute, Laboratory of Hereditary Kidney Diseases, INSERM UMR 1163, F-75015, Paris, France.
[2] Department of Physiology, Necker Hospital, Assistance Publique-Hôpitaux de Paris, Paris, France.
[3] Université de Paris, France.
[4] Institut Necker-Enfants Malades, INSERM U1151, Paris, France.
[5] Department of Pathology, Necker Hospital, Assistance Publique-Hôpitaux de Paris, France.
[6] Renal Department, University Medical Center, Freiburg, Germany.
[7] Laboratory of Biochemistry, Necker Hospital, Assistance Publique-Hôpitaux de Paris, Centre Université de Paris, France.
[8] Department of Pediatry, Necker Hospital, Assistance Publique-Hôpitaux de Paris, France.
[9] Faculty of Medicine, University of Freiburg, Freiburg, Germany.
[10] Center for Biological Signaling Studies (BIOSS), Albert-Ludwigs-University Freiburg, Freiburg, Germany.
* Corresponding author

Corresponding Author

Amandine Viau
Inserm U1163 - Institut Imagine
Laboratory of Inherited Kidney Diseases
Team "nephronophthisis and hypodysplasia"
24 Boulevard du Montparnasse
75015 Paris
France
Tel: +33 1 42 75 43 41
Fax: +33 1 42 75 42 25
Email: amandine.viau@inserm.fr

ABSTRACT (202/250 words)

Renal ciliopathies are the leading cause of inherited kidney failure. In autosomal dominant polycystic kidney disease (ADPKD), mutations in the ciliary gene *PKD1* lead to the induction of CCL2, which promotes macrophage infiltration in the kidney. Whether or not mutations in genes involved in other renal ciliopathies also lead to immune cells recruitment is controversial. Through the parallel analysis of patients derived material and murine models, we investigated the inflammatory components of nephronophthisis (NPH), a rare renal ciliopathy affecting children and adults. Our results show that NPH mutations lead to kidney infiltration by neutrophils, macrophages and T cells. Contrary to ADPKD, this immune cell recruitment does not rely on the induction of CCL2 in mutated cells, which is dispensable for disease progression. Through an unbiased approach, we identified a set of inflammatory cytokines that are upregulated precociously and independently of CCL2 in murine models of NPH. The majority of these transcripts is also upregulated in NPH patient renal cells at a level exceeding those found in common non-immune chronic kidney diseases.

This study reveals that inflammation is a central aspect in NPH and delineates a specific set of inflammatory mediators that likely regulates immune cell recruitment in response to NPH genes mutations.

INTRODUCTION

The primary cilium is a solitary antenna-like structure protruding from the apical surface of renal epithelial tubular cells, that is believed to act as complex macromolecular sensors and signal transducers (1,2).

Renal ciliopathies are inherited disorders caused by mutations in genes encoding proteins that localize to primary cilia (3,4). These renal ciliopathies share common features, including tubular dilation, interstitial fibrosis and loss of tubular cell differentiation. Yet, the spectrum of renal ciliopathies encompasses genetically distinct and phenotypically heterogeneous diseases that manifest from early-childhood to late-adulthood eventually leading to kidney failure. Autosomal dominant polycystic kidney disease (ADPKD), the most common ciliopathy manifesting in adulthood, is characterized by the development of multiple renal cysts resulting in progressive kidney enlargement and kidney function decline. Most ADPKD cases are caused by inactivating mutations in *PKD1*, which encodes polycystin 1 (PC1), that localizes to the ciliary membrane. By contrast, nephronophthisis (NPH), the second most prevalent renal ciliopathy, is a rare autosomal recessive disorder that manifests in children and young adults by enuresis due to impaired urine concentrating ability and progressive kidney function decline. Although some cysts are observed in NPH, cyst burden remains marginal compared to ADPKD, and the kidneys mostly appear small and fibrotic. NPH is a genetically heterogeneous disorder caused by mutations in more than 20 genes identified so far (5). *NPHP1* mutations are the most common genetic cause, accounting for 40-50% of identified causative mutations in NPH (6). Most of the proteins encoded by *NPHP* genes assemble in functional modules that control cilia morphology and gate protein entry and exit to and from the cilia (7,8). Yet, how disruption of these complexes translate into kidney damage is poorly understood.

Primary cilia of renal tubular cells are required for proper kidney development and maintenance (9). Yet, none of the mutations reported in renal ciliopathies abolish ciliogenesis. While renal

tubular cells remain ciliated in renal ciliopathies, they may display either increased or decreased cilia length (10, 11). It is believed that the genetic defects involved in renal ciliopathies adversely affect cilia composition and signaling which results in modifications of tubular cell behavior that, in turn, alter kidney morphology and function. Even outside cilia, NPHP regulate cellular junctions and epithelialization which may also contribute to NPH-associated tubular defects (12).

Lessons gathered from acquired chronic kidney disease (CKD) models indicate that progressive renal scarring involves interplay between tubular, immune and mesenchymal cells that prompts immune cell infiltration, fibroblast activation and nephron loss (13–15).

Concordant evidence has pinpointed an important role of renal inflammation in the progression of ADPKD. Indeed, macrophages infiltrate the kidney of ADPKD patients and mice and promote cyst growth (16). Cilia signaling seems to be directly involved in this process as cilia ablation prevents macrophage recruitment in an orthologous mouse model of ADPKD (17). Mechanistically, cilia positively regulate the expression of the macrophage chemoattractant CCL2 in *Pkd1*-deficient tubular cells both *in vivo* and *in vitro*. Consistently, kidney specific disruption of *Ccl2* or inhibition of the CCL2 receptor reduce cyst burden in *Pkd1* mutant mice (17, 18).

In contrast to ADPKD, the role of immune cells in NPH has received little attention. Recent evidence suggests that renal inflammation may be involved in the disease. First, the inactivation of TLR2, a critical receptor of the immune system, prevents renal damage in an orthologous mouse model of a rare form of NPH caused by a mutation in *Glis2/Nphp7* (*Glis2*$^{lacZ/lacZ}$ mice) (19, 20). Besides, we previously reported that LKB1, a ciliary kinase involved in the control of cell size and metabolism, interacts with NPHP proteins including NPHP1 (17). In human, heterozygous mutation in *STK11*, the gene encoding LKB1, does not lead to NPH but to Peutz-Jeghers syndrome, characterized by benign tumors of the skin and intestine, as well as cancer.

Homozygous mutations in *LKB1* have not been reported in humans, while mice with bi-allelic inactivation of *Lkb1* die at mid-gestation (21). Yet, mice bearing a selective inactivation of *Lkb1* in renal tubules (*Lkb1*$^{\Delta Tub}$ mice) develop a NPH-like phenotype recapitulating the consequences of *NPHP1* loss in humans including impaired urine concentration, thickened tubular basement membranes and fibrosis (17). The relevance of this mouse model to human NPH is not only sustained by the interaction of LKB1 with NPH proteins but also by parallel functions of NPHP1 and LKB1 in tubular cells. Indeed, *in vitro*, both NPHP1 and LKB1 repress the expression of CCL2, while CCL2 upregulation and macrophage recruitment are observed *in vivo* at an early time point of the development of the disease in *Lkb1*$^{\Delta Tub}$ mice (17). Importantly, CCL2 dependent recruitment of immune cells has been repeatedly shown to promote renal fibrosis in different acquired CKD models (15, 21). In contrast to these observations made in NPH mice models, most of the histopathologic studies performed in human NPH did not report immune cells infiltration as a notable feature of the disease (5). Yet, these studies have limitations: they are rare, included a limited number of patients (≤9 patients) and lacked standardized quantitative assessment of renal inflammation.

Considering the paucity and the inconstancy of the data regarding renal inflammation in NPH, we decided to explore the interplay between immune and tubular cells in NPH through a translational approach combining data from transgenic animals and human patients.

RESULTS

Nephronophthisis is associated with macrophage recruitment and enhanced CCL2 expression.

To elucidate the contribution of immune cell recruitment in the phenotype of NPH, we first aimed to assess whether, similar to ADPKD, macrophage infiltration occurs in human NPH. Histology inspection of kidney tissues from NPH patients mostly bearing *NPHP1* mutations, revealed significant infiltration by immune cells (**Figure 1A**). Immunolabelling identified macrophages (CD68-positive cells) as an important contingent of cells infiltrating the kidneys from NPH patients as compared to control individuals (**Figure 1B-C**). As CCL2 has been shown to be the major chemokine responsible for macrophage recruitment in ADPKD, we analyzed primary tubular epithelial cells derived from urine (UREC) of patients bearing *NPHP1* mutations and controls, including both age-matched controls and healthy relatives. UREC derived from *NPHP1* patients showed decreased expression of *NPHP1* mRNA associated with increased expression of *LCN2* transcript, a marker of tubular injury known to correlate with the progression of CKD (**Supplemental Figure 1A-B**). Tubular cells derived from *NPHP1* patients also showed enhanced expression of *CCL2* transcript (**Figure 1D** and **Supplemental Figure 1C**). Consistently, we observed that *NPHP1* patients display a higher urinary excretion rate of CCL2 than controls (**Figure 1E**). Of note, in *NPHP1* patients, CCL2 urinary excretion was not correlated with eGFR (Pearson correlation P=0.218, R^2=0.183) and no difference was observed according to the patient genotype (homozygous deletion *vs* heterozygous compound mutations). Collectively, these data revealed that, similarly to ADPKD, NPH patients show increased renal tubular expression of CCL2 associated with macrophage recruitment.

Tubule-specific *Ccl2* inactivation does not prevent nephronophthisis-like phenotype.

Deletion of *Lkb1* in the distal tubule of mouse kidney cells results in an NPH phenotype associated with CCL2 upregulation and macrophage recruitment (17, 22). To determine if the

deletion of *Ccl2* together with *Lkb1* ameliorates the NPH-like renal disease, we crossed tubule-specific *Lkb1*$^{\Delta tub}$ mice with mice bearing *Ccl2* floxed alleles and compared mice with distal tubular inactivation of *Lkb1* alone (*Lkb1*$^{\Delta tub}$), *Ccl2* alone (*Ccl2*$^{\Delta tub}$) or *Lkb1* and *Ccl2* (*Lkb1*$^{\Delta tub}$; *Ccl2*$^{\Delta tub}$) with littermates controls. At 10 weeks of age, quantitative RT-PCR revealed that *Ccl2* inactivation in distal tubules drastically blunted *Ccl2* induction in *Lkb1* deficient kidneys (**Figure 2A**). Macroscopic inspection revealed irregular kidneys in both *Lkb1*$^{\Delta tub}$ and *Lkb1*$^{\Delta tub}$; *Ccl2*$^{\Delta tub}$ mice associated with reduced kidney size, which was even more pronounced in *Lkb1*$^{\Delta tub}$; *Ccl2*$^{\Delta tub}$ mice (**Figure 2B-C** and **Supplemental Figure 2A-B**). *Lkb1*$^{\Delta tub}$ and *Lkb1*$^{\Delta tub}$; *Ccl2*$^{\Delta tub}$ mice displayed similar urine concentration defect and loss of kidney function (**Figure 2D-F**). Renal histology revealed similar tubular and glomerular basement membranes thickening, interstitial inflammation, fibrosis, and tubular dilation in *Lkb1*$^{\Delta tub}$ and *Lkb1*$^{\Delta tub}$; *Ccl2*$^{\Delta tub}$ mice. Consistently, *Ccl2* inactivation neither affected the upregulation of the tubular injury marker *Lcn2*, nor the extracellular matrix deposition markers *Col1a1* and *Tgfb1*, in *Lkb1* deficient kidneys (**Figure 2G-L**). *Ccl2*$^{\Delta tub}$ animals had normal renal function and histology (**Supplemental Figure 2C-J**). Unexpectedly, contrary to what was observed in *Pkd1* deficient mice (17, 18), *Ccl2* tubular inactivation did not prevent macrophage infiltration of *Lkb1* deficient kidneys as judged by quantification of both F4/80 immunolabelling and *Adgre1* transcript (**Figure 2M-O**). Collectively, these results demonstrate that, while distal tubules represent the major source of renal CCL2 in *Lkb1*$^{\Delta tub}$ mice, CCL2 induction in those cells does not mediate macrophage infiltration of the kidney nor kidney damage.

Early NPH renal disease in mice is associated with a prominent immune signature.

So far, our findings revealed macrophage infiltration in NPH but, as opposed to ADPKD, this recruitment appears independent of tubular CCL2. To approach the mechanisms underlying renal inflammation in NPH in an unbiased manner, we compared microarray-based

transcriptomes from *Lkb1*$^{\Delta Tub}$ and *Glis2*$^{lacZ/lacZ}$ kidneys (17, 19) to controls. Both mouse models recapitulated the features of human NPH: polyuria followed by progressive interstitial fibrosis, tubular basement membrane thickening, tubular dilations and immune cell infiltration (17, 19, 23). Transcriptome datasets were obtained at an early time point of disease development (5 and 4 weeks, respectively) when histological lesions were sparse and renal function decline mild (17, 19). Gene overlap analysis identified 1,262 genes that were commonly deregulated in the two models (**Figure 3A-B** and **Supplemental Table 3**). Gene set enrichment analysis (GSEA) of these genes identified a total of 72 enriched pathways (FDR < 0.05). Among those pathways, 8 were downregulated, consisting mostly of metabolic processes, while 64 biological processes were upregulated (**Supplemental Tables 4-5**). Among the latter, the GSEA revealed a high enrichment in biological processes linked to immune response and inflammation (**Figure 3C**). Network analysis showed a marked association of the common regulated genes with immune pathways (**Figure 3D and Supplemental Figure 3**). This unbiased analysis identified renal inflammation as an early and prominent phenomenon in the course of NPH mouse models.

***Lkb1* tubular inactivation activates multiple chemotactic pathways and drives the recruitment of distinct immune cell populations independently of CCL2.**

To identify specific cytokines that might illuminate CCL2 independent immune cell recruitment in NPH, we matched the common upregulated genes between *Lkb1*$^{\Delta Tub}$ and *Glis2*$^{lacZ/lacZ}$ kidneys with UniProt database. This analysis retrieved 17 pro-inflammatory cytokines, other than CCL2 (**Supplemental Table 6**) that have been implicated in macrophage, neutrophil, T cell and/or dendritic cell chemotaxis. Quantifying these transcripts in kidneys from *Lkb1*$^{\Delta tub}$, *Lkb1*$^{\Delta tub}$; *Ccl2*$^{\Delta tub}$ and control mice, we observed that *Ccl2* disruption had no impact on the up-regulation of these immune mediators in *Lkb1* deficient kidneys (**Figure 4A** and **Supplemental Figure 4**). In line with the different immune cell populations attracted by these cytokines,

immunolabelling demonstrated enhanced neutrophils (Ly-6B.2-positive cells) and T cells (CD3-positive cells) recruitment in both kidneys from *Lkb1*$^{\Delta tub}$ and *Lkb1*$^{\Delta tub}$; *Ccl2*$^{\Delta tub}$ mice as compared to control mice (**Figure 4B-F**). These results uncover a CCL2 independent inflammatory network in NPH-like renal disease.

The identified cytokine signature is not a general feature of renal ciliopathies.

At this point, our findings identified a set of pro-inflammatory cytokines that is expressed early on in the course of NPH renal disease in mice. We next asked whether the observed immune signature was consistent across renal ciliopathies. To address this question, we compared *Lkb1*$^{\Delta tub}$ mice, mimicking human NPH, to an orthologous model of ADPKD, in which post-natal inactivation of *Pkd1* (*Pkd1*$^{\Delta tub}$ mice) results in slow-onset PKD, recapitulating human disease. We focused on early time point of disease development (5 weeks and 10 weeks, respectively). At 5 weeks of age, *Lkb1*$^{\Delta tub}$ mice present scarce renal lesions while *Pkd1*$^{\Delta tub}$ kidneys showed mild tubular dilations 6 weeks after the induction of *Pkd1* recombination, leading to kidney enlargement (**Figure 5A-B**). Quantitative RT-PCR analysis confirmed a marked upregulation of the NPH inflammatory signature in the kidneys from *Lkb1*$^{\Delta tub}$ mice at 5 week of age (**Figure 5C** and **Supplemental Figure 5**). In contrast, while *Pkd1* deficient kidneys displayed a slight but significant induction of CCL2 (**Supplemental Figure 5A**), most of the other cytokines precociously triggered by *Glis2* or *Lkb1* deletion were not induced 6 weeks after the induction of *Pkd1* recombination (**Figure 5C** and **Supplemental Figure 5**). Reanalyzing RNA-seq data from a study involving *Pkd2*$^{\Delta tub}$ mice, another orthologous rodent model of ADPKD (24), further confirmed these results (**Supplemental Figure 6** and **Supplemental Table 7**).

Immunostaining and qPCR analysis demonstrated an infiltration of *Lkb1* deficient kidneys by neutrophils, macrophages and T cells. In contrast, only rare and focal macrophage infiltrates

surrounding expanding cysts were observed in *Pkd1*$^{\Delta tub}$ mice (**Figure 5D-H**). Collectively, these data pinpoint important divergence in the inflammatory processes triggered by *Pkd1* or *Lkb1* deletion. While the inactivation of the former produced tubular dilations associated with focal and CCL2 dependent macrophage recruitment around expanding cysts, the latter is characterized by the up-regulation of multiple cytokines driving kidney infiltration by neutrophils, macrophages and T cells.

Identifying the inflammatory network associated with loss of *NPHP1* function in humans. Considering the distinct immune cell populations infiltrating the kidneys of *Lkb1*$^{\Delta tub}$ mice, we aimed to determine if such phenomena were also found in NPH patients. CD15 and CD3 immunostaining revealed increased neutrophils and T cells recruitment to the renal parenchyma of NPH patients compared to controls (**Figure 6A-B**). In NPH patients, neutrophil infiltrate correlated with the severity of renal lesions evaluated by the interstitial fibrosis and tubular atrophy (IFTA) score (Pearson correlation P=0.02, R^2=0.552) while no correlation was observed with T cells infiltrate (Pearson correlation P=0.69, R^2=0.027). In contrast, these immune cell populations were less abundant in kidney biopsies from patients suffering from acquired non-immune chronic kidney disease (CKD) caused by diabetes or hypertension (**Figure 6A-B**), supporting the notion that a specific inflammatory network delineates human NPH.

To determine if the cytokine network that we identified as features of NPH-like mouse models was relevant to human NPH, we quantified the mRNA abundance of its components in UREC from *NPHP1* patients and controls. As there are no human orthologs for CCL6, 9 and 12, we focused our analysis on the 14 other inflammatory mediators. Indeed, we found 8 transcripts upregulated in human tubular cells with *NPHP1* mutations (*CCL5*, *CXCL1*, *CXCL10*, *CXCL16*, *CXCL17*, *CX3CL1*, *IL1RN* and *LGALS9),* while two were not differentially regulated (*CCL19*

and *IL33*) and 4 were not detected (*CXCL9*, *CXCL12*, *CXCL14*, *IL34)* (**Figure 6C-L**). No difference of these cytokines mRNA expression was observed between age-matched controls and relatives with normal kidney function (**Supplemental Figure 7**). In addition, the mRNA level of CXCL1, CXCL17, IL1RN and LGALS9 were significantly higher in UREC derived from *NPHP1* patients than from patients suffering from other CKD. Of note, CXCL17 mRNA was significantly correlated with eGFR of *NPHP1* patients (**Supplemental Table 8**). CX3CL1, CXCL10 and CXCL16 show the same trend, while not reaching statistical significance (**Figure 6C-L**). Although the molecular mechanisms leading to the upregulation of cytokine expression remain unclear, our *in vitro* data demonstrate that renal tubular cells are the source of cytokine expression in NPH. These data reveal that, in addition to previously described CCL2 upregulation and macrophage infiltration, NPH is characterized by a complex and specific cytokine signature, which is associated with kidney infiltration by neutrophils and T cells.

DISCUSSION

In sharp contrast with the abundant literature regarding the molecular mechanisms of disease progression in ADPKD, insights into the pathophysiology of NPH remain scarce. Despite a growing list of causative gene defects, it is unknown how dysfunction of ciliary NPHP complexes results in the unique renal manifestations of NPH. While some data point to a defect in renal development, a prominent feature is severe progressive fibrosis, resulting in kidney failure during the second decade of life. The study of the molecular pathogenesis of NPH is hampered by the lack of orthologous mouse models recapitulating the fibrotic disease observed in most NPH patients. Indeed, neither *Nphp1*$^{-/-}$ nor *Nphp4*$^{-/-}$ mice develop renal fibrosis (25, 26) and only few mouse models orthologous to rare forms of the disease phenocopy the human pathology (19, 23, 27). In addition, since genetic testing has become more widely available, kidney biopsies are less and less performed in NPH, limiting availability of kidney tissues from patients and insights into the disease.

Renal inflammation has emerged as an important mediator of fibrosis in acquired chronic kidney disease (13). In ADPKD, CCL2 dependent macrophage recruitment promotes disease progression (17, 18). Having previously shown that both NPHP1 and LKB1 repress CCL2 expression *in vitro* and that *Lkb1* inactivation in mice results in an NPH-like phenotype preceded by CCL2 upregulation and macrophage recruitment (17), we first sought to determine if CCL2 induction and macrophage recruitment were also hallmarks of human NPH. In line with the data gathered from *Lkb1*$^{\Delta tub}$ mice, we observed significant macrophage infiltration in kidney biopsies from NPH patients and enhanced CCL2 levels in the urine. We then assessed the role of CCL2 in the *Lkb1*$^{\Delta tub}$ phenotype by inactivating *Ccl2* specifically in tubular cells. Contrary to its effect in ADPKD models (17, 18), *Ccl2* invalidation had no impact on the NPH phenotype of *Lkb1*$^{\Delta tub}$ mice and did not reduce macrophage infiltration, nor inflammatory cytokine expression in *Lkb1* deficient kidneys. Strikingly, CCL2 inactivation even aggravated

kidney size decrease and macrophage infiltration in *Lkb1*$^{\Delta tub}$ mice, suggesting that CCL2 may even exert a limited protective effect on *Lkb1* deficient kidneys.

Beyond ADPKD, CCL2 is instrumental to macrophage recruitment and kidney damage in a range of experimental renal diseases including unilateral ureteric obstruction, acute kidney injury, diabetic nephropathy, subtotal nephrectomy (28) or in response to renal infection (29). Thus, the fact that renal inflammation and macrophage recruitment in *Lkb1*$^{\Delta tub}$ mice is independent of tubular CCL2 suggests that the mechanisms driving renal inflammation in NPH are distinct from those implicated in most kidney diseases. Of note, as we deleted CCL2 only in *Lkb1* deficient distal tubules, we cannot formerly exclude that CCL2 induction in other cell types may be involved in disease progression. Yet, our results clearly rule out the contribution of CCL2 to immune cell recruitment and disease progression in *Lkb1* deficient cells. To get further insight into the nature of renal inflammation in NPH, we analyzed the population of immune cells infiltrating the kidneys in human NPH and *Lkb1*$^{\Delta tub}$ mice. In both case, macrophage infiltration was associated with the recruitment of T cells and neutrophils, by opposition to ADPKD where macrophages are the prominent drivers of inflammation (16–18). To identify the mediators driving early NPH pathology, we analyzed common regulated genes in the transcriptome of *Glis2*$^{lacZ/lacZ}$ and *Lkb1*$^{\Delta tub}$ kidneys, two genetically distinct mouse models of NPH. Unbiased pathway enrichment analysis of their common upregulated genes revealed a striking preponderance of inflammatory processes, pinpointing that early inflammation is a prominent feature of experimental NPH.

Indeed, we found a large number of soluble mediators of immune activation in urinary tubular cells derived from NPH patients. A subset of 7 pro-inflammatory cytokines were specifically upregulated in *NPHP1* UREC and NPH mouse models as compared to urinary tubular cells derived from non-ciliopathy CKD patients: CX3CL1, CXCL1, CXCL10, CXCL16 and

CXCL17, IL1RN and LGALS9. Thus, these cytokines appear more specific of the early renal inflammation observed in NPH.

CXCL1 induces the recruitment of various immune cell types, especially neutrophils, through its receptor CXCR2. The CXCL1/CXCR2/neutrophil axis plays an important role in the pathology of acute kidney inflammation in different mouse models (30–32). Interestingly, we observed concordant neutrophil infiltration in human NPH kidneys and mice, even at an early stage of the disease. In contrast, neutrophil recruitment does not occur in ADPKD (17). As neutrophils are known to promote renal fibrosis (33) it is plausible that CXCL1 mediated neutrophil recruitment contributes to phenotypic changes in NPH.

Our findings add to the recently identified expression of CXCL17 in the kidney (34), the last identified member of the CXC chemokine family in mammals (35, 36). CXCL17 attracts professional antigen presenting cells (37), including macrophages, through its suspected receptor GPR35/CXCR8 (38), even though a second unidentified G protein-coupled receptor may mediate CXCL17-dependent signaling (39). Although very little is known about the role of CXCL17 in the kidney, single-cell RNA sequencing analysis revealed that its expression is enhanced at an early time point in murine tubulointerstitial fibrosis model (34). It is consistent with the increased levels of CXCL17 observed in interstitial pulmonary fibrosis, where it may recruit immune cells that in turn produce pro-inflammatory cytokines (39). Further research may determine if this axis could participate in the pathogenesis of NPH and its fibrotic features.

LGALS9, a mammalian β-galactoside binding lectin (Gal-9), was first isolated from murine embryonic kidney (40). LGALS9 is known to participate in numerous cellular processes including the induction of apoptosis of different immune cells, particularly cytotoxic T lymphocytes when bound to its surface receptor TIM3/HAVCR2 (41). The precise role of LGALS9 in the kidney has not been described so far, however a recent study showed that anti-TIM3 antibody ameliorates kidney injury and decreased macrophage infiltration in ischemic

mouse model (43). This is consistent with a concomitant study that showed increased levels of soluble TIM3 and soluble Gal-9 in the blood of patients with kidney transplantation-related renal dysfunction (43). In addition, upregulation of serum Gal-9 is closely related to glomerular filtration rate decrease in patients with type 2 diabetes (44). Thus, circulating Gal-9 and TIM3 may be useful biomarkers to monitor GFR decline in nephronophthisis. Further studies are needed to assess their function and interplay in the disease. Besides, Gal-9-dependent signaling may participate in switching macrophages from pro-inflammatory M1 phenotype to its anti-inflammatory M2 counterpart, raising the possibility that Gal-9/TIM3 is involved in the polarization of macrophages in NPH (45, 46).

This work identified a specific network of commonly regulated cytokines that represent plausible mediators of immune cell recruitment to NPH kidneys beyond CCL2. We identified inflammation as the predominant signature in two independent models of NPH and we found that this holds true in human patients. As most of the NPH patients studied bear *NPHP1* mutations, we cannot exclude that these findings are specific to NPHP1 patients. Using a non-orthologous mouse model of NPH based on genetic disruption of *Lkb1* may be a limitation of the study. Yet, we confirmed the inflammatory signature identified in *Lkb1*$^{\Delta Tub}$ mice in one of the rare murine orthologous model of NPH leading to renal fibrosis (*Glis2*$^{lacZ/lacZ}$ mice) as well as in UREC derived from *NPHP1* patients. Overall, the similar inflammatory profiles in NPH-like mouse models and in tubular cells derived from NPH patients strengthen our view that *Lkb1*$^{\Delta Tub}$ mice represent a faithful model to study the pathophysiology of NPH. The parallelism between the inflammatory pathways activated in the early diseased kidneys from *Lkb1*$^{\Delta Tub}$ or *Glis2*$^{lacZ/lacZ}$ mice in one hand, and those enriched in the UREC from NPH patients in the other hand, along with the protective effect of TLR2/MYD88 inhibition in *Glis2*$^{lacZ/lacZ}$ mice, suggest causality. However, we cannot exclude that chemokine expression and immune cell recruitment

are innocent bystanders of an undefined process leading to kidney damage in NPH. Certain immune cells may also be protective, such as T lymphocytes in the context of ADPKD (47). This work establishes renal inflammation as a prominent feature of human NPH and identifies specific mediators of this process that are common to NPH mouse models and patients. Addressing the precise function of these mediators in NPH in the future will help to characterize the underlying processes responsible for renal deterioration in this orphan disease and to evaluate inflammation as a potential therapeutic target.

MATERIALS and METHODS

Human kidney tissue specimens

Renal kidney tissues from patients suffering from juvenile nephronophthisis (NPH) were collected from 1973 to 1998. Uneligible kidneys donated for transplantation or kidney from patient suffering from renal disease other than nephronophthisis with minimal histological lesions and collected over the same time period were used as controls. Renal biopsies from patients suffering from diabetic nephropathy or hypertensive nephrosclerosis were used to control for non-specific, chronic kidney disease (CKD) related inflammation. Interstitial fibrosis and tubular atrophy (IFTA) score was evaluated on renal biopsy by a trained pathologist in a blinded fashion. NPH and CKD patient groups were matched according to their IFTA score. Patient data are listed in **Supplemental Table 1**.

Isolation of urine-derived renal epithelial cells (UREC)

Urine samples were collected from *NPHP1* patients, healthy relatives and unrelated controls as well as CKD patients recruited at Necker Hospital (Paris, France) after written informed consent of the donor. Inclusion criteria for affected patients were to suffer from nephronophthisis with known genetic diagnosis. The relatives were the healthy relatives (father/mother/sister) of an included patient. Healthy controls were free from any chronic kidney disease or with normal renal function. CKD patients were suffering from CKD other than renal ciliopathy. Patient data are listed in **Supplemental Table 1**.

Urine-derived renal tubular epithelial cells (primary UREC) were isolated and cultured as previously described (49) with some modifications. Briefly, after centrifugation and washing steps, urine-derived cells were initially cultured for 4 days at 37°C in primary medium containing Dulbecco's Modified Eagle Medium : Nutrient Mixture F-12 (DMEM/F-12) supplemented with 10% fetal bovine serum (16000-036, Gibco), 10% Penicillin-Streptomycin (15140-122, Gibco), 10% Amphotericin B (15290026, Gibco) and 1X REGM™ SingleQuots™

kit (CC-4127, Lonza) to enhance cell survival and adherence. At day 4, primary medium was replaced by a growth medium containing REBM™ (Basal Medium, CC-3191, Lonza) supplemented with 2% fetal bovine serum, 10% Penicillin-Streptomycin, 10% Amphotericin B, 1X REGM™ SingleQuots™ kit and 10 ng/mL rhEGF (R&D system) and was then changed every 2 days. At 80% confluence (7-30 days), $2x10^4$ cells were seeded for 7-24 days until confluence on 12 well plates (353043, Dutscher) for RNA analysis.

Mice

Mice were housed in a specific pathogen-free facility, fed *ad libitum* and housed at constant ambient temperature in a 12-hour day/night cycle. Breeding and genotyping were done according to standard procedures.

Lkb1$^{\Delta Tub}$ mice were previously described (17). *Ccl2*-RFP$^{flox/flox}$ (B6.Cg-Ccl2tm1.1Pame/J, stock number: 016849, C57BL/6J genetic background) were purchased from The Jackson Laboratories and were backcrossed for 2 generations with *Lkb1*$^{\Delta Tub}$ mice. The progeny was then intercrossed to generate mice with tubule-specific *Lkb1* knockout (further referred to as *Lkb1*$^{\Delta Tub}$), *Ccl2* knockout (further referred to as *Ccl2*$^{\Delta Tub}$) and *Lkb1*; *Ccl2* double knockout (further referred to as *Lkb1*$^{\Delta Tub}$; *Ccl2*$^{\Delta Tub}$) on a common mixed C57BL/6J; C57BL/6N genetic background. Littermates lacking *KspCre* transgene were used as controls. Experiments were conducted on both females and males.

Pkd1$^{flox/flox}$ mice (B6.129S4-Pkd1tm2Ggg/J, stock number: 010671, 129.B6 mixed genetic background) were purchased from The Jackson Laboratories and were crossed to Pax8rtTA (Tg(Pax8-rtTA2S*M2)1Koes) and TetOCre (Tg(tetO-cre)1Jaw) mice to generate an inducible tubule-specific *Pkd1* knockout (further referred to as i*Pkd1*$^{\Delta Tub}$) as previously described (17). To induce recombination, mice received doxycycline (Abcam, ab141091) in drinking water (2mg/mL with 5% sucrose, protected from light) from post-natal day 28 (P28) to P42.

Littermates lacking either TetOCre or Pax8rtTA were used as controls. Experiments were conducted on males.

Quantitative PCR

Total RNAs were obtained from human UREC or mouse kidneys using RNeasy Mini Kit (Qiagen) and reverse transcribed using SuperScript II Reverse Transcriptase (Life Technologies) or High Capacity cDNA Reverse Transcription Kit (Applied Biosystems) according to the manufacturer's protocol. Quantitative PCR were performed with iTaq™ Universal SYBR® Green Supermix (Bio-Rad) on a CFX384 C1000 Touch (Bio-Rad). *Hprt, Ppia, Rpl13, Sdha and Tbp* were used as normalization controls (50). Each biological replicate was measured in technical duplicates. The primers used for qRT-PCR are listed in Supplemental Table 2.

CCL2 ELISA

For the quantification of urinary CCL2 excretion, urine specimens were collected and centrifuged at 1500 g for 10 minutes at 4°C within 4h of collection. The supernatants were collected and stored at -80°C. Frozen aliquots of urine supernatants were thawed at room temperature immediately before the ELISA. The samples were used with a 2-fold dilution and were tested in duplicates. CCL2 levels in urine specimens were quantified using Human CCL2/MCP-1 Quantikine® ELISA Kit (R&D systems, DCP00) according to the manufacturer's instructions. The plate was read using a Multiskan Sky plate reader. The optical densities were derived from 4-parameter logistic regression of the standard curve. Measurement of creatinine in urine was performed in the same samples using IDMS-standardized enzymatic method on C16000 Architect analyzer (Abbott Diagnostic). The results were normalized to the urinary creatinine level. Indeed, normalization by the urinary creatinine levels avoids the pitfall of concentration or dilution of urine.

Morphological Analysis

Human kidney biopsies were fixed in alcohol formalin and acetic acid and paraffin embedded, 4µm sections were stained with periodic acid-Schiff (PAS). PAS-stained full size images were recorded using a whole slide scanner Nanozoomer 560 (Hamamatsu) coupled to NDPview software (Hamamatsu).

Mouse kidneys were fixed in 4% paraformaldehyde, embedded in paraffin, and 4µm sections were stained with PAS or Picrosirius Red. Stained full size images were recorded using a whole slide scanner Nanozoomer 2.0 (Hamamatsu) equipped with a 20x/0.75 NA objective coupled to NDPview software (Hamamatsu). Histology score was evaluated by an independent observer in a blinded fashion assessing the overall lesions of the whole kidney section stained with PAS. Six scores were defined ranging from score 1 normal kidney architecture to score 6 associating tubular atrophy, tubular basement thickening and interstitial cell infiltration.

Urine and Plasma Analyses

8-hour urine samples were obtained from mice housed in individual boxes without access to water and food. Body weight and urine excretion were measured. Urine osmolality was measured with a freezing point depression osmometer (Micro-Osmometer from Knauer or OSMOMAT 3000basic from Gonotec). Retro-orbital blood was collected from anaesthetized mice. Plasma blood urea nitrogen (BUN) was measured using urea kit (LT-UR; Labor&Technik, Eberhard Lehmann GmbH) according to the manufacturer's instructions.

Immunohistochemistry

<u>For human kidney sections</u>

An automated IHC stainer BOND-III (Leica Biosystems) was used. Briefly, 4µm sections of paraffin-embedded human kidney biopsies were submitted to the appropriate antigen retrieval. Then, sections were incubated with CD68 (Dako, M0814, 1:3,000), CD15 (Beckam Coulter, NIM0165, 1:200) or CD3 (Dako, A0452, 1:200) antibodies. Peroxide blocking, post primary, DAB chromogen and hematoxylin counterstaining was performed automatically using Bond

polymer refine detection kit (Leica Biosystems, DS9800). The degree of interstitial cell infiltration was determined using immunostaining targeting macrophages (CD68), neutrophils (CD15) and T lymphocytes (CD3). Slides were scanned with a whole slide scanner Nanozoomer 560 (Hamamatsu). Randomly selected microscopic fields (x200) representative of the entire cortical surface were scored. The degree of cell infiltrate was quantified using ImageJ software. For CD3 and CD68, the area of DAB staining was measured after color deconvolution and intensity thresholding of the images and visualized as the ratio of DAB surface to cortical surface on each microscopic field. For CD15, the number of CD15-positive interstitial cells was quantified manually in a blinded fashion and was expressed as a ratio per mm^2.

For mouse kidney sections

Macrophage staining: 4µm sections of paraffin-embedded mouse kidneys were incubated for 20 min at 95°C in citrate buffer (Zytomed, ZUCD28) followed by avidin/biotin blocking (Vector, SP-2001). Sections were incubated with F4/80 antibody (Clone Cl:A3-1, Bio-Rad, MCA497R, 1:100) followed by biotinylated antibody (Vector, BA-4001, 1:200), HRP-labeled streptavidin (Southern Biotech, 7100-05, 1:2,000) and 3-3′-diamino-benzidine-tetrahydrochloride (DAB, Dako, K3468) revelation.

Neutrophil staining: 4µm sections of paraffin-embedded mouse kidneys were submitted to antigen retrieval for 20 min at 95°C in citrate buffer followed by incubation with Ly-6B.2 antibody (Abcam, ab53457, 1:100). Sections were incubated with HRP-labeled secondary antibody (Vector, PI-9400, 1:200) and DAB revelation.

T cell staining: 4µm sections of paraffin-embedded mouse kidneys were incubated for 20 min at 95°C in Tris-EDTA pH9 buffer followed by avidin/biotin blocking. Sections were incubated with CD3 antibody (Abcam, ab16669, 1:100) followed by biotinylated antibody (GE

Healthcare, RPN1004V, 1:200), HRP-labeled streptavidin (Southern Biotech, 7100-05, 1:2,000) and DAB revelation.

Full size images were recorded using a whole slide scanner Nanozoomer 2.0 coupled to NDPview software. Stained area was measured with ImageJ software from full size kidney images and visualized as the ratio of stained DAB surface to total kidney section area. For neutrophil quantification in Figure 5, since neutrophils are rare and focal in 5 weeks old mice, we counted manually the number of foci in whole kidney section. The number of foci per kidney section was scaled to the surface of the section. Foci were defined as 4 or more neutrophils surrounding a tubule. For all quantification, glomerular and non-specific intra-tubular staining were removed from the analysis.

Comparative microarray data analysis

Processing of data was carried out using R v3.6.0, RStudio and R package dplyr v1.0.1. Renal transcriptomic datasets from 5 weeks old *Lkb1*$^{\Delta Tub}$ and 4 weeks old *Glis2*$^{lacZ/lacZ}$ mouse models (17, 19) were compared. While transcriptomic dataset from *Lkb1*$^{\Delta Tub}$ mice was established by our team (GSE86011) (17), we downloaded from the GEO database (https://www.ncbi.nlm.nih.gov/geo/) the expression matrix of mRNAs expressions in the kidneys of *Glis2*$^{lacZ/lacZ}$ mice under the accession number GSE6113 (19). Probe IDs in the expression matrix were matched with the corresponding gene IDs in the lookup table (GPL2897) to identify the expression of each mRNA. To assess the common regulated genes between the two mouse models, *Lkb1*$^{\Delta Tub}$ dataset was filtered out according to false discovery rate (FDR, Benjamini-Hochberg procedure) < 0.05 to obtain a list of 1991 differentially expressed genes (DEGs). Then, *Glis2*$^{lacZ/lacZ}$ dataset (23957 genes) was matched with this DEGs list, and the genes whose expression varies in the same way were considered as the common regulated genes (Supplemental Table 3).

GSEA, networking and visualization

Subsequently, Gene Set Enrichment Analysis (GSEA) approach was applied to the 1262 common regulated genes identified using GSEA software v4.0.0 (Broad Institute) set for 000 gene set permutations. The enrichment involved the « biological process » classification of the Gene Ontology downloaded from MSigDB v7.1 (C5-BP). Up- and down-regulated pathways are listed in Tables S4-S5. Pathways with FDR < 0.05 were considered significant. R package ggplot2 was used to present the more significant up- and down-regulated pathways. Cytoscape software v3.0 and Cytoscape applications EnrichmentMap v3.3.0 (edge cutoff threshold set to 0.5) and WordCloud v3.1.3 were used for pathway clustering and pathway network visualization (51). Pathway clusters have been hand-annotated.

Identification of common upregulated cytokines

To identify common upregulated cytokines, the 823 common upregulated genes were matched with lists of genes obtained from the UniProt database (https://www.uniprot.org/) using the following keywords: « cytokine », « secreted » and « immune/inflammation ». Genes that were linked to the 3 keywords are listed in Supplemental Table 6.

Heatmaps of the expression of the identified cytokines from 5 weeks old *Lkb1*$^{\Delta Tub}$ and 10 weeks old *Pkd2*$^{\Delta Tub}$ were compared. The *Pkd2*$^{\Delta Tub}$ log-normalized expression matrix was downloaded from GEO under the accession number GSE149739 (24). Differential expression testing between groups was performed using limma v3.42.2. Heatmaps were generated using the R package pheatmap v1.0.12 (note: heatmaps show Z-scores computed from the expression matrix for each gene, thus presenting expression levels with relatives equal means for each gene). Expression levels of the identified cytokines are listed in Supplemental Table 7. Finally, the heatmap in Figures 4c and 5c displays Z-scores computed on the expression levels of the identified cytokines, measured by qPCR. The corresponding qPCR results are listed in Figures S4 and S5.

Statistical analysis

Data were expressed as means. Differences between groups were evaluated using Mann-Whitney test when only two groups were compared. When testing more comparisons, Kruskal-Wallis test was used when the groups do not meet normal distribution otherwise one-way ANOVA followed when significant ($P < 0.05$) by the Tukey-Kramer test was used. The statistical analysis was performed using GraphPad Prism V8 software. All image analysis and mouse phenotypic analysis were performed in a blinded fashion.

Study approval

The human kidney tissue specimens belonging to the Imagine Biocollection are declared to the French Minister of Research under the number DC-2020-3994 and approved by the French Ethics committee for research at Assistance Publique-Hôpitaux de Paris (CERAPHP) under the IRB registration number #00011928. The urine study was approved by the French National Committee for the Protection of Persons (CPP) under the ID-RCB number 2016-A00541-50 and is kept in full accordance with the principles of the Declaration of Helsinki and Good Clinical Practice guidelines.

All animal experiments were conducted according to the guidelines of the National Institutes of Health *Guide for the Care and Use of Laboratory Animals*, as well as the German and French laws for animal welfare, and were approved by regional authorities (Regierungspräsidium Freiburg G-16/27 and Ministère de l'Enseignement, de la Recherche et de l'Innovation APAFIS#2020090715389782).

ACKNOWLEDGEMENTS

The authors thank Dr. Alexandre Benmerah for critical appraisal of the manuscript.

We thank the technicians from the mouse histology and breeding facilities (S.F.R Necker INSERM US24, Paris, France) and the department of Pathology (Necker Hospital, Paris, France) for technical assistance. We are grateful to the patients and their families for their participation. We thank Pauline Krug, Olivia Boyer, Nathalie Biebuyck, Saoussen Krid, Marina Charbit, Romain Berthaud and Guillaume Lezmi (Pediatric Nephrology, Necker Hospital, AP-HP, Paris, France), Aurélie Hummel (Adult Nephrology, Necker Hospital, AP-HP, Paris, France), Amélie Lezmi Ryckewaert and Sophie Taque (Pediatric Hematology and Oncology, Hôpital Universitaire, Rennes, France), Odile Boespflug-Tanguy (Centre de Compétence des Leucodystrophies et Leucoencéphalopathies de Cause Rare, Pôle Femme et Enfant, Hôpital Estaing, Centre Hospitalier Universitaire de Clermont-Ferrand, Clermont-Ferrand, France), Jérôme Harambat and Brigitte Llanas (Department of Pediatrics, Bordeaux University Hospital, Bordeaux, France), Bruno Ranchin (Pediatric Nephrology, Centre Hospitalier Universitaire de Lyon, Bron, France), Elodie Merieau (Centre Hospitalier Régional Universitaire de Tours, Tours, France), Marc Fila (Centre Hospitalier Universitaire de Montpellier, Montpellier, France) and Tory Kalman (Semmelweis University, Budapest, Hungary) who helped the follow-up of patients. We thank Corinne Antignac and Laurence Heidet (Department of Genetics, Necker Hospital, AP-HP, Paris, France) for genetic diagnostic. We thank the Department of Clinical Research at Imagine Institute with the sponsorship team that facilitates and structures the set-up of the clinical research projects and the investigation team that prepares and ensures the follow-up of the clinical trials.

Marceau Quatredeniers and Amandine Viau were supported by a public grant “RHU-C’IL-LICO” overseen by the Agence Nationale de la Recherche (grant number: ANR-17-RHUS-0002), Frank Bienaimé was supported by EMBO (grant number: ALTF 927-2013), E.

Wolfgang Kuehn was supported by Deutsche Forschungsgemeinschaft (grant numbers: KU1504/7-1 and KU1504/8-1), Sophie Saunier was supported by the Institut National de la Santé et de la Recherche Médicale (INSERM), the Ministère de l'Education Nationale de la Recherche et de la Technologie (MRT), by a State funding from the Agence Nationale de la Recherche (grant references: ANR-10-IAHU-01, ANR-17-RHUS-0002).

CONFLICT OF INTEREST STATEMENT

The authors declare that they have no conflict of interest.

REFERENCES

1. Reiter, J.F., Blacque, O.E. and Leroux, M.R. (2012) The base of the cilium: Roles for transition fibres and the transition zone in ciliary formation, maintenance and compartmentalization. *EMBO Rep.*, **13**, 608–618.
2. Satir, P. (2017) CILIA: Before and after. CILIA: Before and after. *Cilia* **(2017)** .
3. Braun, D.A. and Hildebrandt, F. (2017) Ciliopathies. *Cold Spring Harb. Perspect. Biol.*
4. Devlin, L.A. and Sayer, J.A. (2019) Renal ciliopathies. *Curr. Opin. Genet. Dev.*, **56**, 49–60.
5. Srivastava, S., Molinari, E., Raman, S. and Sayer, J.A. (2018) Many genes-one disease? Genetics of nephronophthisis (NPHP) and NPHP-associated disorders. Many genes-one disease? Genetics of nephronophthisis (NPHP) and NPHP-associated disorders. *Front. Pediatr.* **(2018)** .
6. König, J., Kranz, B., König, S., Schlingmann, K.P., Titieni, A., Tönshoff, B., Habbig, S., Pape, L., Häffner, K., Hansen, M., *et al.* (2017) Phenotypic spectrum of children with nephronophthisis and related ciliopathies. *Clin. J. Am. Soc. Nephrol.*, **12**, 1974–1983.
7. Sang, L., Miller, J.J., Corbit, K.C., Giles, R.H., Brauer, M.J., Otto, E.A., Baye, L.M., Wen, X., Scales, S.J., Kwong, M., *et al.* (2011) Mapping the NPHP-JBTS-MKS protein network reveals ciliopathy disease genes and pathways. *Cell*, **145**, 513–528.
8. Toriyama, M., Lee, C., Taylor, S.P., Duran, I., Cohn, D.H., Bruel, A.L., Tabler, J.M., Drew, K., Kelly, M.R., Kim, S., *et al.* (2016) The ciliopathy-associated CPLANE proteins direct basal body recruitment of intraflagellar transport machinery. *Nat. Genet.*, **48**, 648–656.
9. Lin, F., Hiesberger, T., Cordes, K., Sinclair, A.M., Goldstein, L.S.B.B., Somlo, S. and Igarashi, P. (2003) Kidney-specific inactivation of the KIF3A subunit of kinesin-II

inhibits renal ciliogenesis and produces polycystic kidney disease. *Proc. Natl. Acad. Sci. U. S. A.*, **100**, 5286–5291.

10. Hopp, K., Ward, C.J., Hommerding, C.J., Nasr, S.H., Tuan, H.F., Gainullin, V.G., Rossetti, S., Torres, V.E. and Harris, P.C. (2012) Functional polycystin-1 dosage governs autosomal dominant polycystic kidney disease severity. *J. Clin. Invest.*
11. Davis, E.E., Zhang, Q., Liu, Q., Diplas, B.H., Davey, L.M., Hartley, J., Stoetzel, C., Szymanska, K., Ramaswami, G., Logan, C. V., *et al.* (2011) TTC21B contributes both causal and modifying alleles across the ciliopathy spectrum. *Nat. Genet.*
12. Delous, M., Hellman, N.E., Gaudé, H.M., Silbermann, F., Le Bivic, A., Salomon, R., Antignac, C. and Saunier, S. (2009) Nephrocystin-1 and nephrocystin-4 are required for epithelial morphogenesis and associate with PALS1/PATJ and Par6. *Hum. Mol. Genet.*, **18**, 4711–4723.
13. Andrade-Oliveira, V., Foresto-Neto, O., Watanabe, I.K.M., Zatz, R. and Câmara, N.O.S. (2019) Inflammation in renal diseases: New and old players. *Front. Pharmacol.*
14. Bienaimé, F., Muorah, M., Yammine, L., Burtin, M., Nguyen, C., Baron, W., Garbay, S., Viau, A., Broueilh, M., Blanc, T., *et al.* (2016) Stat3 Controls Tubulointerstitial Communication during CKD. *J. Am. Soc. Nephrol.*, **27**.
15. Kitagawa, K., Wada, T., Furuichi, K., Hashimoto, H., Ishiwata, Y., Asano, M., Takeya, M., Kuziel, W.A., Matsushima, K., Mukaida, N., *et al.* (2004) Blockade of CCR2 ameliorates progressive fibrosis in kidney. *Am J Pathol*, **165**, 237–246.
16. Karihaloo, A., Koraishy, F., Huen, S.C., Lee, Y., Merrick, D., Caplan, M.J., Somlo, S. and Cantley, L.G. (2011) Macrophages Promote Cyst Growth in Polycystic Kidney Disease. *J. Am. Soc. Nephrol.*, **22**, 1809–1814.
17. Viau, A., Bienaimé, F., Lukas, K., Todkar, A.P.A.P., Knoll, M., Yakulov, T.A.T.A., Hofherr, A., Kretz, O., Helmstädter, M., Reichardt, W., *et al.* (2018) Cilia-localized

LKB 1 regulates chemokine signaling, macrophage recruitment, and tissue homeostasis in the kidney . *EMBO J.*, **37**, 1–21.

18. Cassini, M.F., Kakade, V.R., Kurtz, E., Sulkowski, P., Glazer, P., Torres, R., Somlo, S. and Cantley, L.G. (2018) Mcp1 Promotes Macrophage-Dependent Cyst Expansion in Autosomal Dominant Polycystic Kidney Disease. .
19. Attanasio, M., Uhlenhaut, N.H., Sousa, V.H., O'Toole, J.F., Otto, E., Anlag, K., Klugmann, C., Treier, A.C., Helou, J., Sayer, J.A., *et al.* (2007) Loss of GLIS2 causes nephronophthisis in humans and mice by increased apoptosis and fibrosis. *Nat. Genet.*, **39**, 1018–1024.
20. Jin, H., Zhang, Y., Liu, D., Wang, S.S., Ding, Q., Rastogi, P., Purvis, M., Wang, A., Elhadi, S., Ren, C., *et al.* (2019) Innate Immune Signaling Contributes to Tubular Cell Senescence in the Glis2 Knockout Mouse Model of Nephronophthisis. *Am. J. Pathol.*, **190**, 176–189.
21. Ollila, S. and Mäkelä, T.P. (2011) The tumor suppressor kinase LKB1: Lessons from mouse models. *J. Mol. Cell Biol.*, **3**, 330–340.
22. Braga, T.T., Correa-Costa, M., Silva, R.C., Cruz, M.C., Hiyane, M.I., da Silva, J.S., Perez, K.R., Cuccovia, I.M. and Camara, N.O.S. (2017) CCR2 contributes to the recruitment of monocytes and leads to kidney inflammation and fibrosis development. *Inflammopharmacology*, 1–9.
23. Han, S.H., Malaga-DIeguez, L., Chinga, F., Kang, H.M., Tao, J., Reidy, K. and Susztak, K. (2016) Deletion of Lkb1 in renal tubular epithelial cells leads to CKD by altering metabolism. *J. Am. Soc. Nephrol.*
24. Kim, Y.-S., Kang, H.S., Herbert, R., Beak, J.Y., Collins, J.B., Grissom, S.F. and Jetten, A.M. (2008) Kruppel-Like Zinc Finger Protein Glis2 Is Essential for the Maintenance of Normal Renal Functions. *Mol. Cell. Biol.*, **28**, 2358–2367.

25. Zhang, C., Balbo, B., Ma, M., Zhao, J., Tian, X., Kluger, Y. and Somlo, S. (2020) Cyclin-Dependent Kinase 1 Activity Is a Driver of Cyst Growth in Polycystic Kidney Disease. *J. Am. Soc. Nephrol.*

26. Jiang, S.T., Chiou, Y.Y., Wang, E., Lin, H.K., Lee, S.P., Lu, H.Y., Wang, C.K.L., Tang, M.J. and Li, H. (2008) Targeted disruption of Nphp1 causes male infertility due to defects in the later steps of sperm morphogenesis in mice. *Hum. Mol. Genet.*, **17**, 3368–3379.

27. Won, J., de Evsikova, C.M., Smith, R.S., Hicks, W.L., Edwards, M.M., Longo-Guess, C., Li, T., Naggert, J.K. and Nishina, P.M. (2011) NPHP4 is necessary for normal photoreceptor ribbon synapse maintenance and outer segment formation, and for sperm development. *Hum. Mol. Genet.*, **20**, 482–496.

28. Airik, R., Slaats, G.G., Guo, Z., Weiss, A.C., Khan, N., Ghosh, A., Hurd, T.W., Bekker-Jensen, S., Schrøder, J.M., Elledge, S.J., *et al.* (2014) Renal-retinal ciliopathy gene Sdccag8 regulates DNA damage response signaling. *J. Am. Soc. Nephrol.*, **25**, 2573–2583.

29. Akli Ayoub, M., Zhang, Y., Kelly, R.S., See, H.B., M Johnstone, E.K., McCall, E.A., Williams, J.H., Kelly, D.J. and G Pfleger, K.D. (2015) Functional Interaction between Angiotensin II Receptor Type 1 and Chemokine (C-C Motif) Receptor 2 with Implications for Chronic Kidney Disease. .

30. Berry, M.R., Mathews, R.J., Ferdinand, J.R., Kuper, C., Jing, C., Loudon, K.W., Wlodek, E., Dennison, T.W., Neuhofer, W. and Clatworthy, M.R. (2017) Renal Sodium Gradient Orchestrates a Dynamic Antibacterial Defense Zone In Brief Sodium gradient guides the migration of innate immune cells in the kidney during infections. Article Renal Sodium Gradient Orchestrates a Dynamic Antibacterial Defense Zone. *Cell*, **170**, 860–874.

31. Liu, P., Li, X., Lv, W. and Xu, Z. (2020) Inhibition of CXCL1-CXCR2 axis ameliorates cisplatin-induced acute kidney injury by mediating inflammatory response. *Biomed. Pharmacother.*

32. Ranganathan, P., Jayakumar, C., Manicassamy, S. and Ramesh, G. (2013) CXCR2 knockout mice are protected against DSS-colitis-induced acute kidney injury and inflammation. *Am. J. Physiol. - Ren. Physiol.*

33. Brown, H.J., Lock, H.R., Wolfs, T.G.A.M., Buurman, W.A., Sacks, S.H. and Robson, M.G. (2007) Toll-like receptor 4 ligation on intrinsic renal cells contributes to the induction of antibody-mediated glomerulonephritis via CXCL1 and CXCL2. *J. Am. Soc. Nephrol.*

34. Wang, H., Gao, M., Li, J., Sun, J., Wu, R., Han, D., Tan, J., Wang, J., Wang, B., Zhang, L., *et al.* (2019) MMP-9-positive neutrophils are essential for establishing profibrotic microenvironment in the obstructed kidney of UUO mice. *Acta Physiol.*, **227**, 1–13.

35. Conway, B., O'Sullivan, E., Cairns, C., O'Sullivan, J., Simpson, D., Salzano, A., Connor, K., Ding, P., Humphries, D., Stewart, K., *et al.* (2020) Kidney single-cell atlas reveals myeloid heterogeneity in progression and regression of kidney disease. *J. Am. Soc. Nephrol.*

36. Pisabarro, M.T., Leung, B., Kwong, M., Corpuz, R., Frantz, G.D., Chiang, N., Vandlen, R., Diehl, L.J., Skelton, N., Kim, H.S., *et al.* (2006) Cutting Edge: Novel Human Dendritic Cell- and Monocyte-Attracting Chemokine-Like Protein Identified by Fold Recognition Methods. *J. Immunol.*

37. Weinstein, E.J., Head, R., Griggs, D.W., Sun, D., Evans, R.J., Swearingen, M.L., Westlin, M.M. and Mazzarella, R. (2006) VCC-1, a novel chemokine, promotes tumor growth. *Biochem. Biophys. Res. Commun.*

38. Xiao, S., Xie, W. and Zhou, L. (2020) Mucosal chemokine CXCL17: What is known and not known. Mucosal chemokine CXCL17: What is known and not known. *Scand. J. Immunol.* **(2020)** .

39. Maravillas-Montero, J.L., Burkhardt, A.M., Hevezi, P.A., Carnevale, C.D., Smit, M.J. and Zlotnik, A. (2015) Cutting Edge: GPR35/CXCR8 Is the Receptor of the Mucosal Chemokine CXCL17. *J. Immunol.*, **194**, 29–33.

40. Choreño-Parra, J.A., Thirunavukkarasu, S., Zúñiga, J. and Khader, S.A. (2020) The protective and pathogenic roles of CXCL17 in human health and disease: Potential in respiratory medicine. The protective and pathogenic roles of CXCL17 in human health and disease: Potential in respiratory medicine. *Cytokine Growth Factor Rev.* **(2020)** .

41. Wada, J. and Kanwar, Y.S. (1997) Identification and characterization of galectin-9, a novel β- galactoside-binding mammalian lectin. *J. Biol. Chem.*

42. Fujita, K., Iwama, H., Oura, K., Tadokoro, T., Samukawa, E., Sakamoto, T., Nomura, T., Tani, J., Yoneyama, H., Morishita, A., *et al.* (2017) Cancer therapy due to apoptosis: Galectin-9. Cancer therapy due to apoptosis: Galectin-9. *Int. J. Mol. Sci.* **(2017)** .

43. Guo, Y., Zhang, J., Lai, X., Chen, M. and Guo, Y. (2018) Tim-3 exacerbates kidney ischaemia/reperfusion injury through the TLR-4/NF-κB signalling pathway and an NLR-C4 inflammasome activation. *Clin. Exp. Immunol.*

44. Li, Y.M., Shi, Y.Y., Li, Y., Yan, L., Tang, J.T., Bai, Y.J., Wu, X.J., Dai, B., Zou, Y.G. and Wang, L.L. (2018) Soluble Tim-3 and Gal-9 are associated with renal allograft dysfunction in kidney transplant recipients: A cross-sectional study. *Int. Immunopharmacol.*

45. Kurose, Y., Wada, J., Kanzaki, M., Teshigawara, S., Nakatsuka, A., Murakami, K., Inoue, K., Terami, T., Katayama, A., Watanabe, M., *et al.* (2013) Serum galectin-9

levels are elevated in the patients with type 2 diabetes and chronic kidney disease. *BMC Nephrol.*

46. Jung, S.H., Hwang, J.H., Kim, S.E., Kim, Y.K., Park, H.C. and Lee, H.T. (2017) Human galectin-9 on the porcine cells affects the cytotoxic activity of M1-differentiated THP-1 cells through inducing a shift in M2-differentiated THP-1 cells. *Xenotransplantation*.
47. Zhang, W., Zhang, Y., He, Y., Wang, X. and Fang, Q. (2019) Lipopolysaccharide mediates time-dependent macrophage M1/M2 polarization through the Tim-3/Galectin-9 signalling pathway. *Exp. Cell Res.*
48. Kleczko, E.K., Marsh, K.H., Tyler, L.C., Furgeson, S.B., Bullock, B.L., Altmann, C.J., Miyazaki, M., Gitomer, B.Y., Harris, P.C., Weiser-Evans, M.C.M., *et al.* (2018) CD8+ T cells modulate autosomal dominant polycystic kidney disease progression. *Kidney Int.*
49. Ajzenberg, H., Slaats, G.G., Stokman, M.F., Arts, H.H., Logister, I., Kroes, H.Y., Renkema, K.Y., van Haelst, M.M., Terhal, P.A., van Rooij, I.A., *et al.* (2015) Non-invasive sources of cells with primary cilia from pediatric and adult patients. *Cilia*, **4**.
50. Vandesompele, J., De Preter, K., Pattyn, F., Poppe, B., Van Roy, N., De Paepe, A. and Speleman, F. (2002) Accurate normalization of real-time quantitative RT-PCR data by geometric averaging of multiple internal control genes. *Genome Biol.*, **3**, 1–12.
51. Reimand, J., Isserlin, R., Voisin, V., Kucera, M., Tannus-Lopes, C., Rostamianfar, A., Wadi, L., Meyer, M., Wong, J., Xu, C., *et al.* (2019) Pathway enrichment analysis and visualization of omics data using g:Profiler, GSEA, Cytoscape and EnrichmentMap. *Nat. Protoc.*

LEGENDS TO FIGURES

Figure 1

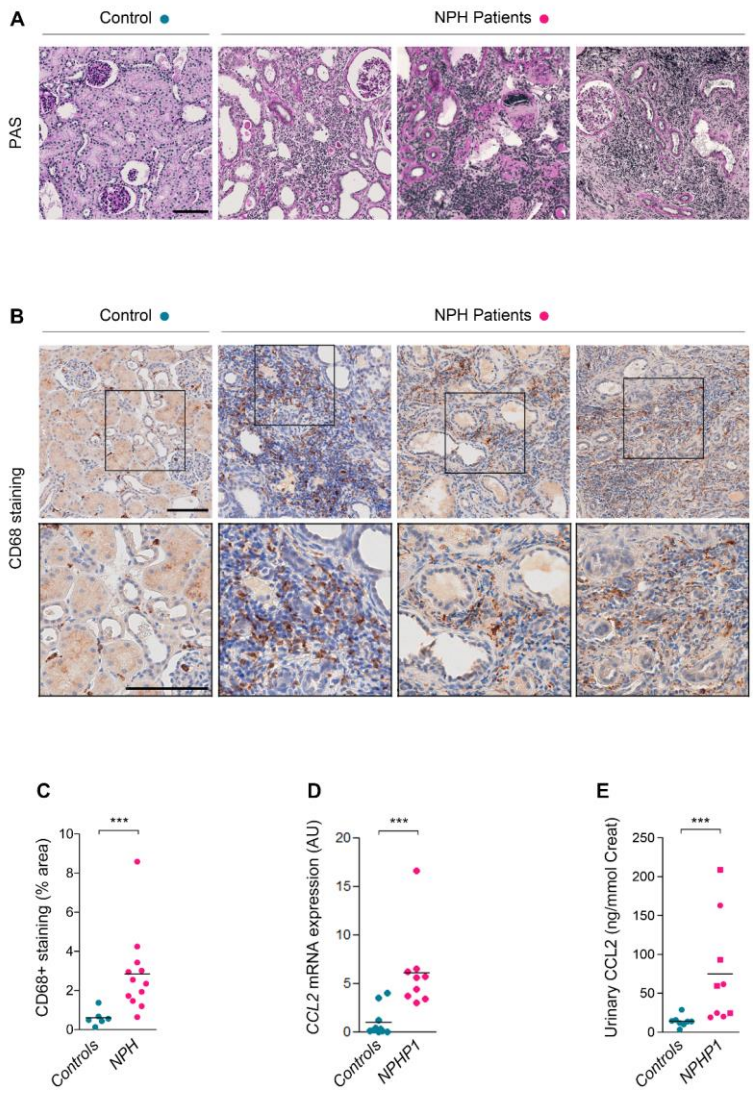

Figure 1. Human nephronophthisis is associated with renal inflammation, macrophage infiltration and CCL2 induction. (A) Representative images of Periodic Acid–Schiff (PAS) stained kidney biopsies from control and 3 NPH patients. Scale bar: 100µm. **(B)** Representative images of CD68 (macrophages) immunostaining in kidney biopsies from control and 3 NPH patients. Scale bar: 100µm. **(C)** Quantification of CD68-positive staining area in kidney sections from control and NPH patients**. (D)** *CCL2* mRNA expression in primary UREC derived from urine from controls (Controls) and *NPHP1* patients (NPHP1). **(E)** Urinary CCL2 secretion in controls and *NPHP1* patients. Filled circles indicate *NPHP1* patients bearing homozygous deletion while filled squares indicate those with heterozygous compound mutations. **(C-E)** Each dot represents one individual. Bars indicate mean. Mann-Whitney t test, *** $P < 0.001$. AU: arbitrary unit.

Figure 2

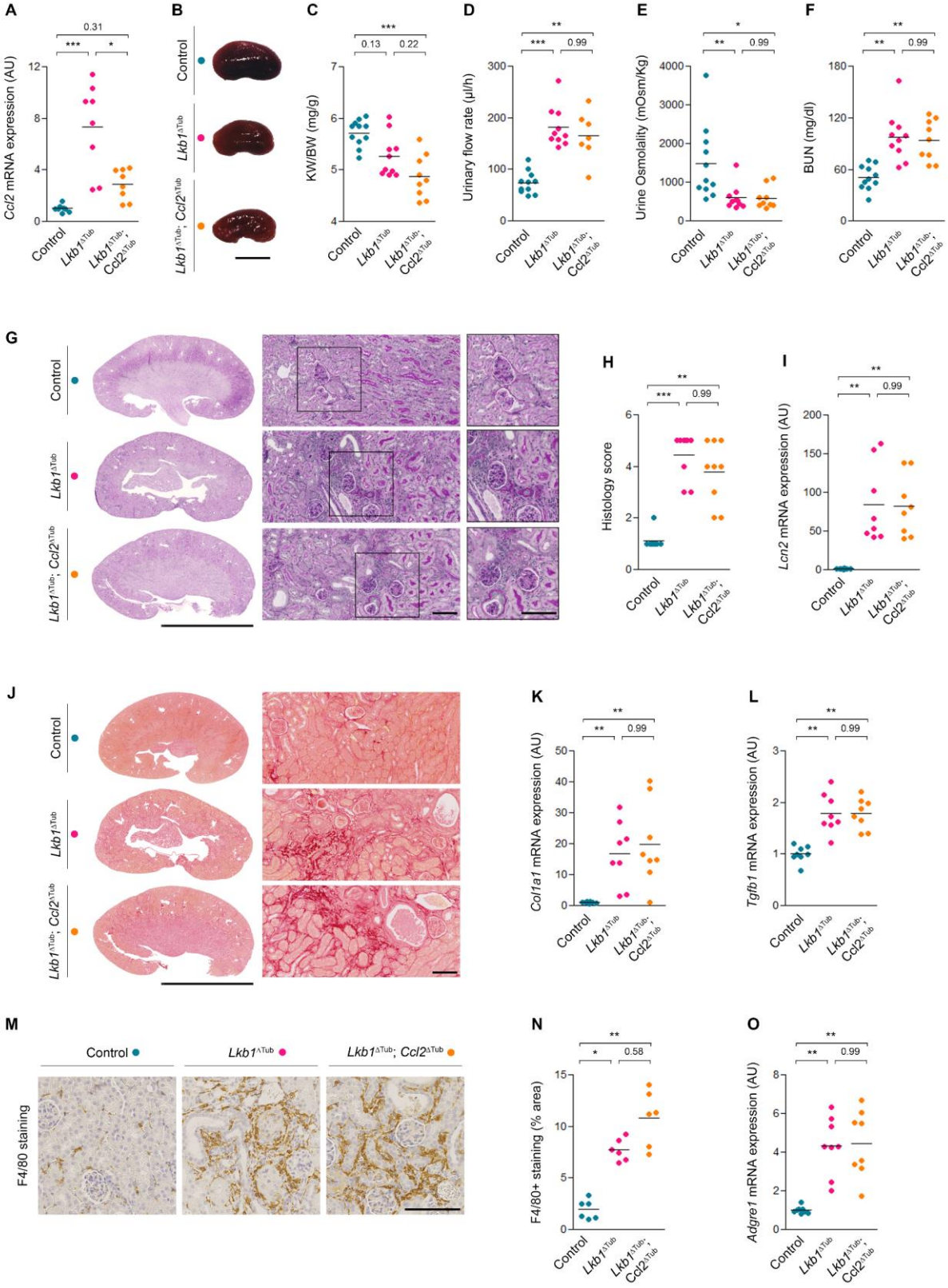
A
Ccl2 mRNA expression (AU)
0.31
***
*
Control
Lkb1ΔTub
Lkb1ΔTub; Ccl2ΔTub
B
Control
Lkb1ΔTub
Lkb1ΔTub; Ccl2ΔTub
C
KW/BW (mg/g)
***
0.13
0.22
D
Urinary flow rate (µl/h)
**
***
0.99
E
Urine Osmolality (mOsm/Kg)
*
**
0.99
F
BUN (mg/dl)
**
**
0.99
G
H
Histology score
**
***
0.99
I
Lcn2 mRNA expression (AU)
**
**
0.99
J
K
Col1a1 mRNA expression (AU)
**
**
0.99
L
Tgfb1 mRNA expression (AU)
**
**
0.99
M
F4/80 staining
N
F4/80+ staining (% area)
**
*
0.58
O
Adgre1 mRNA expression (AU)
**
**
0.99

Figure 2. Tubule specific *Ccl2* inactivation does not prevent renal lesion development nor macrophage infiltration of *Lkb1* deficient kidneys. (A) *Ccl2* mRNA expression in kidneys from control, *Lkb1*$^{\Delta Tub}$ and *Lkb1*$^{\Delta Tub}$; *Ccl2*$^{\Delta Tub}$ mice at 10 weeks. **(B)** Representative kidneys from control, *Lkb1*$^{\Delta Tub}$ and *Lkb1*$^{\Delta Tub}$; *Ccl2*$^{\Delta Tub}$ mice. Scale bar: 5 mm. **(C)** Kidney weight to body weight ratio (KW/BW). **(D-E)** Urinary flow rate (D) and urine osmolality (E). **(F)** Plasma blood urea nitrogen (BUN). **(G-H)** Representative PAS stained kidney sections (G) and histology scores (H) from control, *Lkb1*$^{\Delta Tub}$ and *Lkb1*$^{\Delta Tub}$; *Ccl2*$^{\Delta Tub}$ mice. Scale bars: 5mm (left panel), 100µm (middle, right panel). **(I)** *Lcn2* mRNA expression in kidneys from the same animals. **(J)** Representative sirius red stained kidney sections of the same animals Scale bars: 5mm (left panel), 100µm (right panel). **(K-L)** *Col1a1* (K) and *Tgfb1* (L) mRNA expression in kidneys from control, *Lkb1*$^{\Delta Tub}$ and *Lkb1*$^{\Delta Tub}$; *Ccl2*$^{\Delta Tub}$ mice. **(M-N)** Representative images (M) and quantification (N) of F4/80 (macrophages) immunostaining in the same animals. Scale bar: 100µm. **(O)** *Adgre1* mRNA expression in kidneys from control, *Lkb1*$^{\Delta Tub}$ and *Lkb1*$^{\Delta Tub}$; *Ccl2*$^{\Delta Tub}$ mice. **(A, C-F, H-I, K-L, N-O)** Each dot represents one individual mouse. All mice were 10 weeks old. Bars indicate mean. Kruskal-Wallis test, * $P < 0.05$, ** $P < 0.01$, *** $P < 0.001$. AU: arbitrary unit.

Figure 3

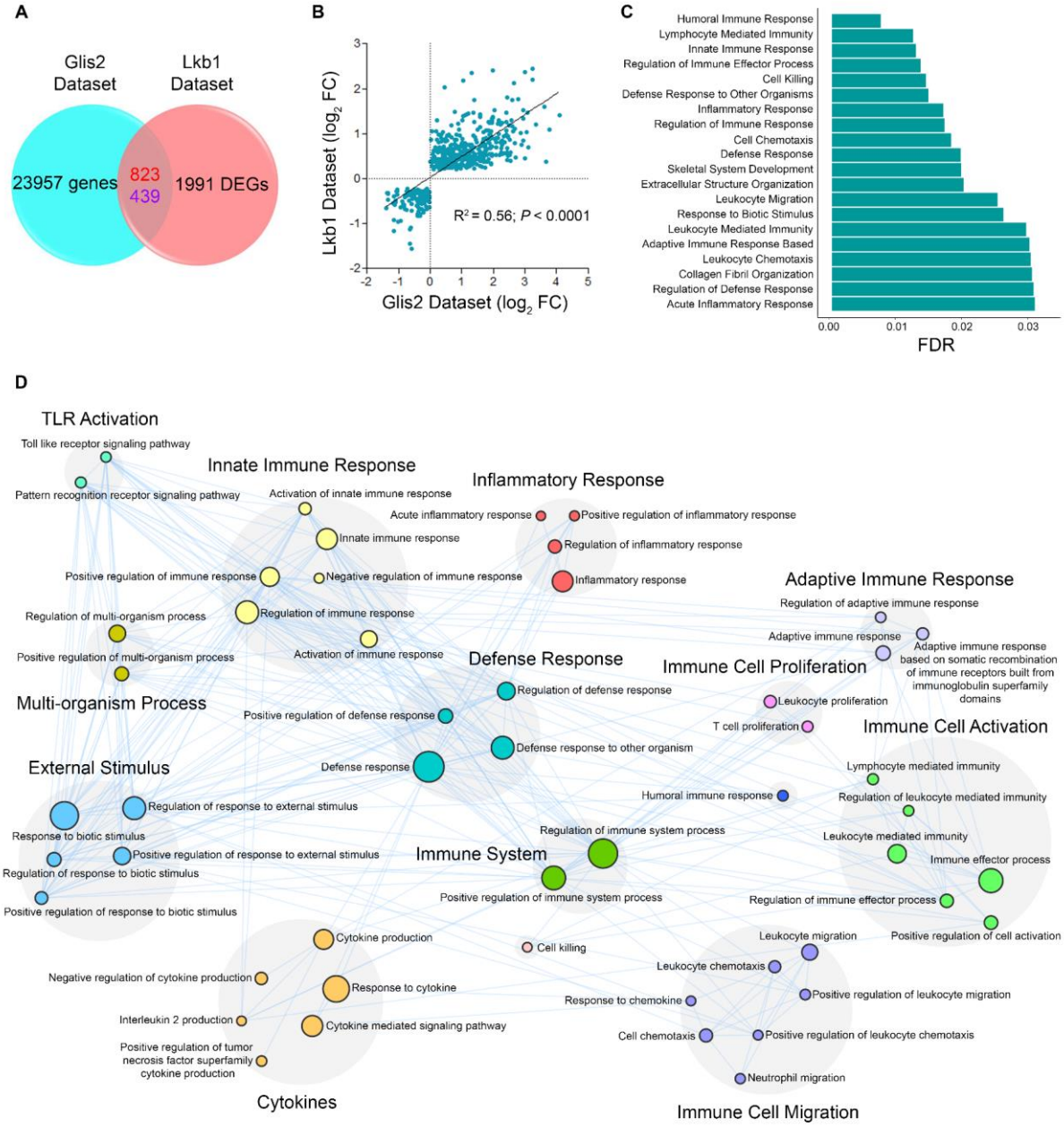
A
Glis2 Dataset
Lkb1 Dataset
23957 genes
823
439
1991 DEGs
B
Lkb1 Dataset (log2 FC)
Glis2 Dataset (log2 FC)
R² = 0.56; P < 0.0001
C
Humoral Immune Response
Lymphocyte Mediated Immunity
Innate Immune Response
Regulation of Immune Effector Process
Cell Killing
Defense Response to Other Organisms
Inflammatory Response
Regulation of Immune Response
Cell Chemotaxis
Defense Response
Skeletal System Development
Extracellular Structure Organization
Leukocyte Migration
Response to Biotic Stimulus
Leukocyte Mediated Immunity
Adaptive Immune Response Based
Leukocyte Chemotaxis
Collagen Fibril Organization
Regulation of Defense Response
Acute Inflammatory Response
FDR
D
TLR Activation
Toll like receptor signaling pathway
Pattern recognition receptor signaling pathway
Innate Immune Response
Activation of innate immune response
Innate immune response
Inflammatory Response
Acute inflammatory response
Positive regulation of inflammatory response
Regulation of inflammatory response
Inflammatory response
Positive regulation of immune response
Negative regulation of immune response
Regulation of immune response
Activation of immune response
Regulation of multi-organism process
Positive regulation of multi-organism process
Multi-organism Process
Defense Response
Regulation of defense response
Positive regulation of defense response
Defense response to other organism
Defense response
External Stimulus
Regulation of response to external stimulus
Response to biotic stimulus
Positive regulation of response to external stimulus
Regulation of response to biotic stimulus
Positive regulation of response to biotic stimulus
Immune System
Regulation of immune system process
Positive regulation of immune system process
Adaptive Immune Response
Regulation of adaptive immune response
Adaptive immune response
Adaptive immune response based on somatic recombination of immune receptors built from immunoglobulin superfamily domains
Immune Cell Proliferation
Leukocyte proliferation
T cell proliferation
Immune Cell Activation
Lymphocyte mediated immunity
Humoral immune response
Regulation of leukocyte mediated immunity
Leukocyte mediated immunity
Immune effector process
Regulation of immune effector process
Positive regulation of cell activation
Cytokine production
Cell killing
Negative regulation of cytokine production
Response to cytokine
Interleukin 2 production
Cytokine mediated signaling pathway
Positive regulation of tumor necrosis factor superfamily cytokine production
Cytokines
Leukocyte migration
Leukocyte chemotaxis
Response to chemokine
Positive regulation of leukocyte migration
Cell chemotaxis
Positive regulation of leukocyte chemotaxis
Neutrophil migration
Immune Cell Migration

Figure 3. Comparative renal transcriptome analysis in *Glis2* mutant mice and kidney-specific *Lkb1* deficient mice. (A) Venn diagram showing intersection between *Glis2*$^{lacZ/lacZ}$ (left; 23957 genes) and *Lkb1*$^{\Delta Tub}$ (right; 1991 differentially expressed genes (DEGs) according to FDR < 0.05) datasets. Red numbers: upregulated; blue numbers: downregulated. **(B)** Jointly up- and down-regulated genes in *Lkb1*$^{\Delta Tub}$ mice (Lkb1 dataset) and *Glis2*$^{lacZ/lacZ}$ mice (Glis2 dataset). Genes with FDR < 0.01 are represented. Pearson correlation $R^2 = 0.56$, $P < 0.0001$. **(C)** Gene set enrichment analysis (GSEA) on the 1262 common regulated genes revealed 72 pathways overrepresented (FDR < 0.05); the 20 most significantly upregulated are presented. See also **Supplemental Tables 4-5**. **(D)** Summarized subnetwork representation of significantly enriched Biological Processes GO terms (MSigDB v7.1, C5-BP) linked to immune/inflammatory pathways derived from the GSEA of the 1262 common regulated genes in *Glis2*$^{lacZ/lacZ}$ and *Lkb1*$^{\Delta Tub}$ kidneys. Nodes are connected according to a similarity score > 0.5, and pathway clusters are hand-annotated according to the most representative GO-BP terms. The full network representation is available in **Supplemental Figure 3**.

Figure 4

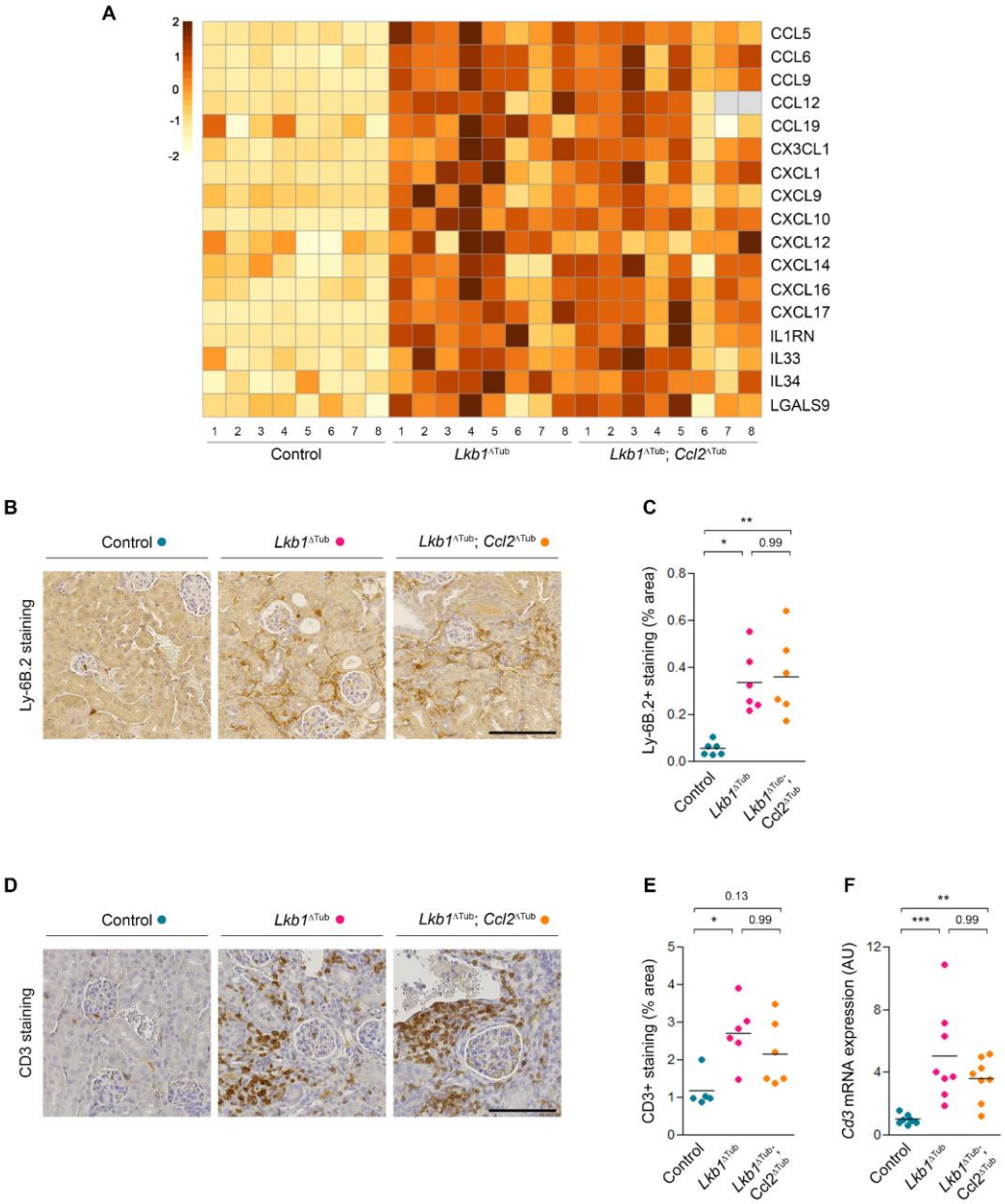
A
CCL5
CCL6
CCL9
CCL12
CCL19
CX3CL1
CXCL1
CXCL9
CXCL10
CXCL12
CXCL14
CXCL16
CXCL17
IL1RN
IL33
IL34
LGALS9
Control
Lkb1ΔTub
Lkb1ΔTub; Ccl2ΔTub
B
Ly-6B.2 staining
C
Ly-6B.2+ staining (% area)
D
CD3 staining
E
CD3+ staining (% area)
F
Cd3 mRNA expression (AU)

Figure 4. NPH cytokine signature and immune cell infiltrations occurred independently of CCL2 in *Lkb1* deficient mice. **(A)** Heatmap showing Z-scores computed on mRNA expression measured by qPCR of the indicated cytokines in kidneys from 10 weeks old control, *Lkb1*$^{\Delta Tub}$ and *Lkb1*$^{\Delta Tub}$; *Ccl2*$^{\Delta Tub}$ mice. See also **Supplemental Figure 4**. **(B-C)** Representative images (B) and quantification (C) of Ly-6B.2 (neutrophils) immunostaining of kidney sections from control, *Lkb1*$^{\Delta Tub}$ and *Lkb1*$^{\Delta Tub}$; *Ccl2*$^{\Delta Tub}$ mice at 10 weeks. Scale bar: 100µm. **(D-E)** Representative images (D) and quantification (E) of CD3 (T lymphocytes) immunostaining of kidney sections from the same animals. Scale bar: 100µm. **(F)** *Cd3* mRNA expression in kidneys from the same animals. **(B, D-E)** Each dot represents one individual mouse. Bars indicate mean. Kruskal-Wallis test, * $P < 0.05$, *** $P < 0.001$. AU: arbitrary unit.

Figure 5

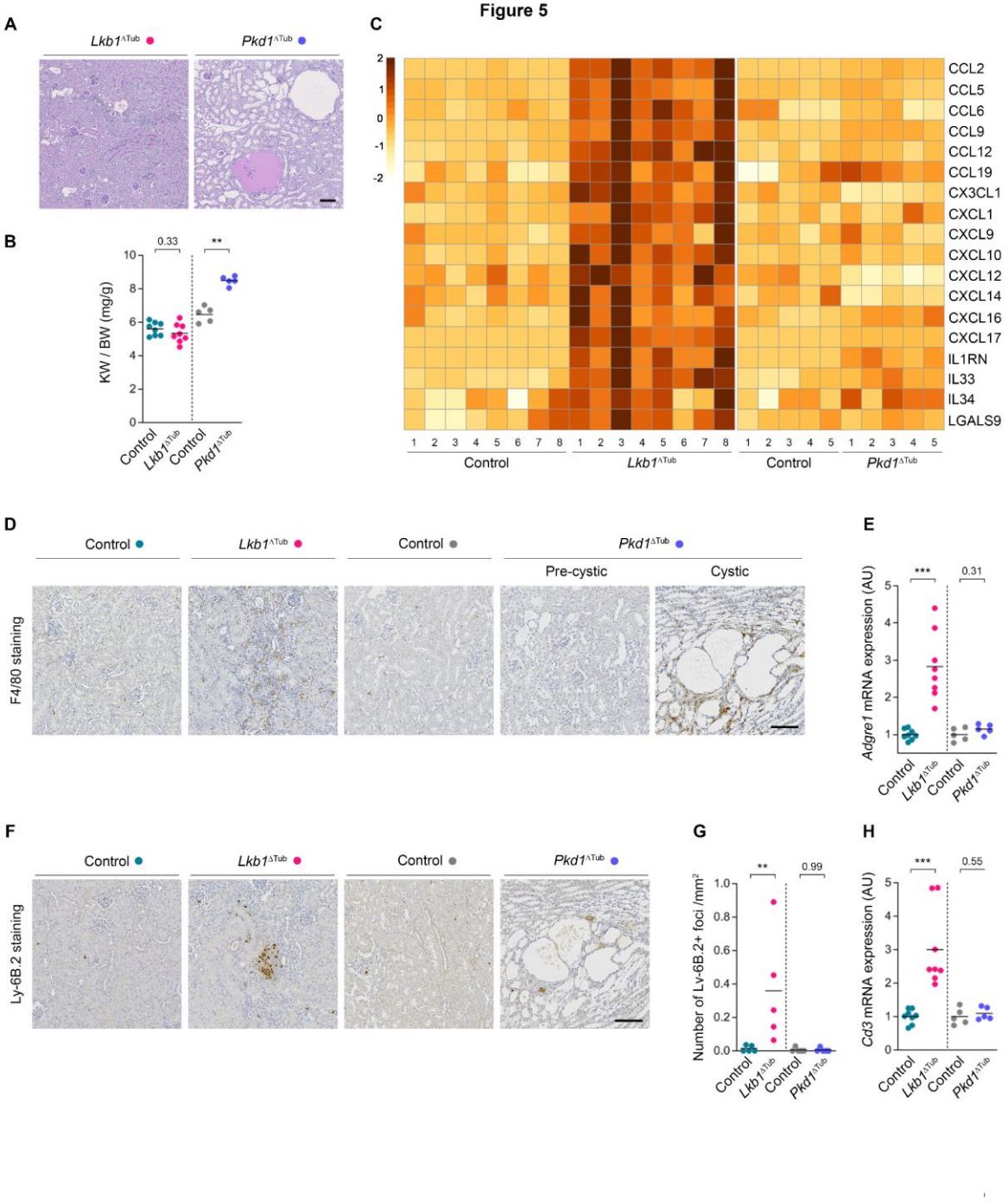
A
Lkb1ΔTub
Pkd1ΔTub
B
0.33
**
KW / BW (mg/g)
Control
Lkb1ΔTub
Control
Pkd1ΔTub
C
CCL2
CCL5
CCL6
CCL9
CCL12
CCL19
CX3CL1
CXCL1
CXCL9
CXCL10
CXCL12
CXCL14
CXCL16
CXCL17
IL1RN
IL33
IL34
LGALS9
Control
Lkb1ΔTub
Control
Pkd1ΔTub
D
Control
Lkb1ΔTub
Control
Pkd1ΔTub
Pre-cystic
Cystic
F4/80 staining
E
***
0.31
Adgre1 mRNA expression (AU)
F
Control
Lkb1ΔTub
Control
Pkd1ΔTub
Ly-6B.2 staining
G
**
0.99
Number of Ly-6B.2+ foci /mm²
H
***
0.55
Cd3 mRNA expression (AU)

Figure 5. The early inflammatory signature of NPH is not a common feature of renal ciliopathies. (A) Representative PAS stained kidney sections from 5 weeks old male *Lkb1*$^{\Delta Tub}$ and 10 weeks old male *Pkd1*$^{\Delta Tub}$ mice. Scale bars: 100µm. **(B)** Kidney weight to body weight ratio (KW/BW) from 5 weeks old control and *Lkb1*$^{\Delta Tub}$ animals and 10 weeks old control and *Pkd1*$^{\Delta Tub}$ mice. **(C)** Heatmap showing Z-scores computed on mRNA expression measured by qPCR of the indicated cytokines in kidneys from 5 weeks old control and *Lkb1*$^{\Delta Tub}$ mice, and 10 weeks old control and *Pkd1*$^{\Delta Tub}$ mice. See also **Supplemental Figure 5**. **(D)** Representative images of F4/80 (macrophages) immunostaining of kidney sections from 5 weeks old control and *Lkb1*$^{\Delta Tub}$ mice and 10 weeks old control and *Pkd1*$^{\Delta Tub}$ mice. Scale bar: 100µm. **(E)** *Adgre1* mRNA expression in the same mice. **(F-G)** Representative images (F) and quantification (G) of Ly-6B.2 (neutrophils) immunostaining of kidney sections from 5 weeks old control and *Lkb1*$^{\Delta Tub}$ mice and 10 weeks old control and *Pkd1*$^{\Delta Tub}$ mice. Scale bar: 100µm. **(H)** *Cd3* mRNA expression in kidneys from the same animals. **(B, E, G-H)** Each dot represents one individual mouse. Bars indicate mean. Mann-Whitney test, ** $P < 0.01$, *** $P < 0.001$. AU: arbitrary unit. All animals were males.

Figure 6

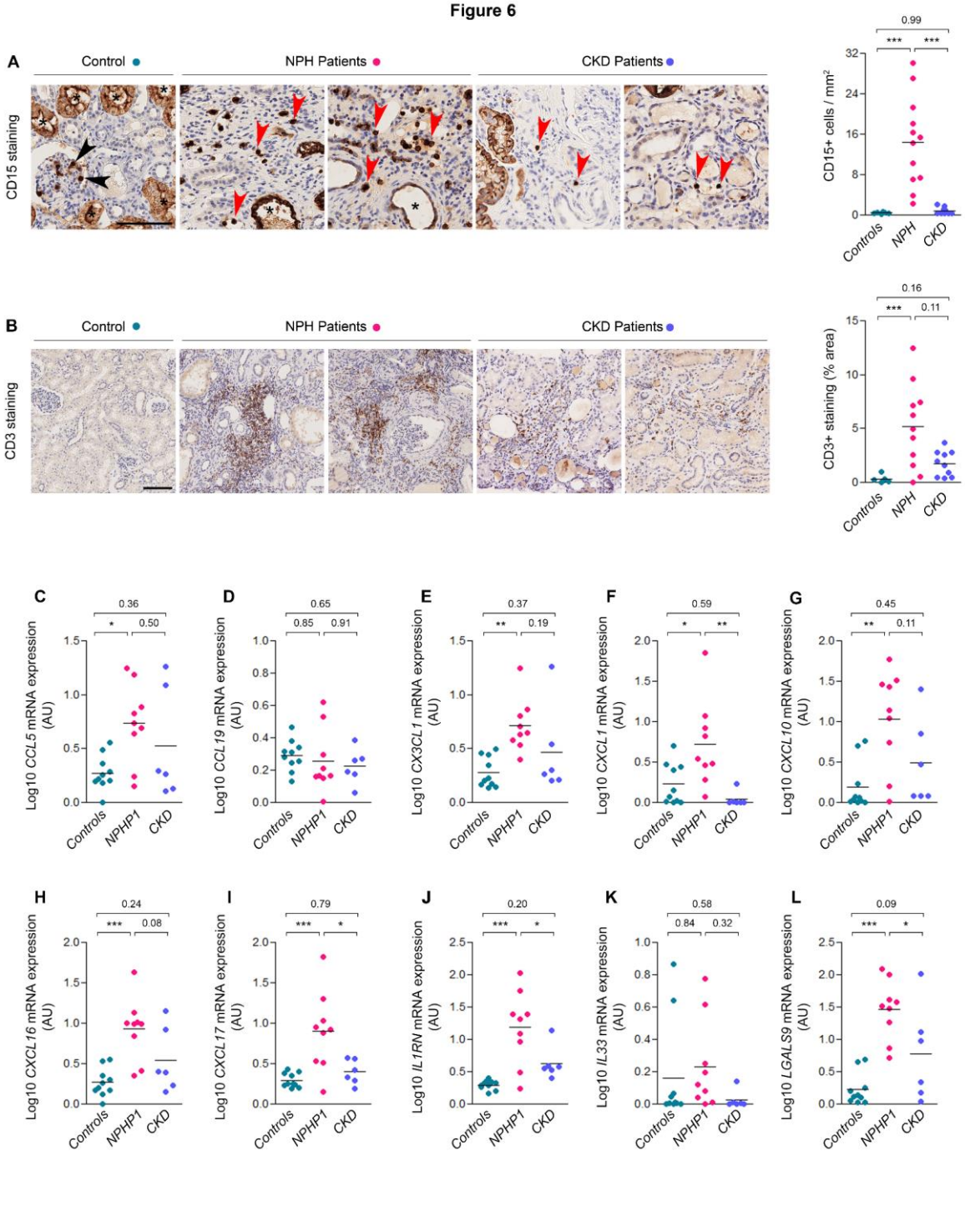
A
Control
NPH Patients
CKD Patients
CD15 staining
CD15+ cells / mm²
0.99
***
***
Controls
NPH
CKD
B
CD3 staining
CD3+ staining (% area)
0.16
***
0.11
C
Log10 CCL5 mRNA expression (AU)
0.36
*
0.50
D
Log10 CCL19 mRNA expression (AU)
0.65
0.85
0.91
E
Log10 CX3CL1 mRNA expression (AU)
0.37
**
0.19
F
Log10 CXCL1 mRNA expression (AU)
0.59
*
**
G
Log10 CXCL10 mRNA expression (AU)
0.45
**
0.11
H
Log10 CXCL16 mRNA expression (AU)
0.24
***
0.08
I
Log10 CXCL17 mRNA expression (AU)
0.79
***
*
J
Log10 IL1RN mRNA expression (AU)
0.20
***
*
K
Log10 IL33 mRNA expression (AU)
0.58
0.84
0.32
L
Log10 LGALS9 mRNA expression (AU)
0.09
***
*
Controls
NPHP1
CKD

Figure 6. The immune signature of murine NPH is also prominent in human NPH. (A) Representative images and quantification of CD15 (neutrophils) immunostaining of kidney biopsies from control, NPH and chronic kidney disease (CKD) patients. Scale bar: 100µm. Asterisk: unspecific tubular staining, black arrow: intravascular neutrophils in a glomerulus, red arrow, interstitial neutrophils. **(B)** Representative images and quantification of CD3 (T lymphocytes) immunostaining of kidney biopsies from control, NPH and CKD patients. Scale bar: 100µm. **(C-L)** *CCL5* (C), *CCL19* (D), *CX3CL1* (E), *CXCL1* (F), *CXCL10* (G), *CXCL16* (H), *CXCL17* (I), *IL1RN* (J), *IL33* (K), *LGALS9* (L) mRNA expression expressed in Log10 in primary UREC from controls (Controls), *NPHP1* patients (NPHP1) and non-ciliopathy CKD patients (CKD). **(A-L)** Each dot represents one individual. Bars indicate mean. **(A-B)** Kruskal-Wallis test, *** $P < 0.001$. **(C-L)** One-way ANOVA followed by Tukey-Kramer test, * $P < 0.05$, ** $P < 0.01$, *** $P < 0.001$. AU: arbitrary unit.

ABBREVIATIONS

ADPKD: autosomal dominant polycystic kidney disease

NPH: nephronophthisis

RC: renal ciliopathies